Decay properties of states populated with the ^{207}Pb$(n,n'\gamma)$ reaction and weak coupling in ^{207}Pb

M. Kadi, P. E. Garrett,* Minfang Yeh,† and S. W. Yates
University of Kentucky, Lexington, Kentucky 40506-0055

T. Belgya
Institute of Isotopes of the Hungarian Academy of Sciences, Budapest H-1525, Hungary

A. M. Oros-Peusquens‡ and K. Heyde
Institute for Theoretical Physics, Vakgroep Subatomaire en Stralingsfysica, Proeftuinstraat 86, B-9000 Gent, Belgium
(Received 24 February 1999; published 17 February 2000)

The properties of states in ^{207}Pb populated with the $(n,n'\gamma)$ reaction have been studied. γ-ray excitation functions, angular distributions, and coincidences have been measured, and the lifetimes of many excited states were determined with the Doppler-shift attenuation method. A sextuplet of states near 3.2 MeV is interpreted as resulting from weak-coupling of the $\nu f_{5/2}^{-1}$ first excited state of ^{207}Pb with the octupole phonon of the ^{208}Pb core. A number of $E1$ transitions have been identified, and their reduced transition probabilities have been examined. The properties of low-lying levels in ^{207}Pb have been studied in the framework of the particle-core coupling model.

PACS number(s): 21.10.Re, 21.10.Tg, 23.20.−g, 25.40.Fq

I. INTRODUCTION

Low-lying collective excitations in odd-A spherical nuclei can arise from particle-vibration coupling of particle (or hole) configurations to the vibrational core of the closed-shell neighboring even-even nucleus. According to the weak-coupling model, a multiplet of levels with spins and parities determined by the rules of angular momentum coupling will be located at an energy equal to the sum of the single-particle and the vibrational core states [1]. To a large extent the collective properties of the levels are determined by the characteristics of the corresponding phonon states in the neighboring nucleus. If the phonon state, for example the 3^- octupole-phonon level in ^{208}Pb, has an enhanced $B(E3)$ value for its decay, the particle-(or hole)phonon coupled excitation in the odd-A nucleus will also exhibit enhanced $E3$ transitions.

Examples of phonon excitations coupled to the ground-state configurations of odd-A nuclei are commonplace. The classic examples of weak-coupled states are the well-known $3^-\otimes h_{9/2}$ and $3^-\otimes p_{1/2}^{-1}$ multiplets in ^{209}Bi and ^{207}Pb, respectively. However, even though these are ''textbook'' examples of weak coupling, the properties of these states are often not well established. Configurations involving phonons coupled to excited single-particle states are rarer.

Recently, a state suggested as the 0^+ member of the two-phonon octupole quartet in ^{208}Pb was identified by observing a cascade of two $E3$ transitions from that state [2]. Because $E1$ transitions are expected to dominate the decays of the remaining members of the quartet, knowledge of the $E1$ decays of states formed by coupling a neutron hole or proton particle to the 3^- octupole phonon of ^{208}Pb proved important in identifying candidates for the 2^+ and 4^+ members of the quartet [3]. The transition rates of $E1$ decays from collective excitations in nuclei near closed shells are, therefore, of considerable current interest; however, the number of experimentally determined $E1$ decay rates for such states are limited.

An extensive investigation of ^{207}Pb has been performed with the $(n,n'\gamma)$ reaction. The primary goals of this work were to provide detailed experimental information about the low-lying levels of ^{207}Pb, to locate additional octupole-coupled states in ^{207}Pb, and to obtain information about $E1$ transition rates. In addition, the properties of low-lying states in ^{207}Pb have been examined within the particle-core coupling model (PCM).

II. EXPERIMENTAL METHODS AND DATA ANALYSIS

γ-ray spectroscopy following the inelastic neutron scattering (INS) reaction was used to study the low-lying, low-spin level structure of ^{207}Pb. The INS reaction at low energy offers unique advantages in studying the low-lying states in nuclei. The statistical population of levels via the compound nucleus mechanism provides a means for studying states of varied nuclear structure. Also, the absence of a Coulomb barrier in this reaction permits excitation with low-energy neutrons, eliminating problems associated with feeding from higher-lying levels.

The ^{207}Pb$(n,n'\gamma)$ experiments were performed at the University of Kentucky 7.0 MV Van de Graaff accelerator. The ^{3}H$(p,n)^3$He reaction was used for neutron production. The proton beam was pulsed with a width of approximately 1 ns and a repetition rate of 1.875 MHz. The scattering sample consisted of 40.916 g of lead metal, enriched to 92.78% in ^{207}Pb, in the form of a cylinder with a diameter of

*Present address: Lawrence Livermore National Laboratory, L-414, P.O. Box 808, Livermore, CA 94550.
†Present address: Department of Chemistry, Washington State University, Pullman, WA 99164.
‡Permanent address: Institute for Nuclear Physics and Engineering, Bucharest-Magurele, Romania.

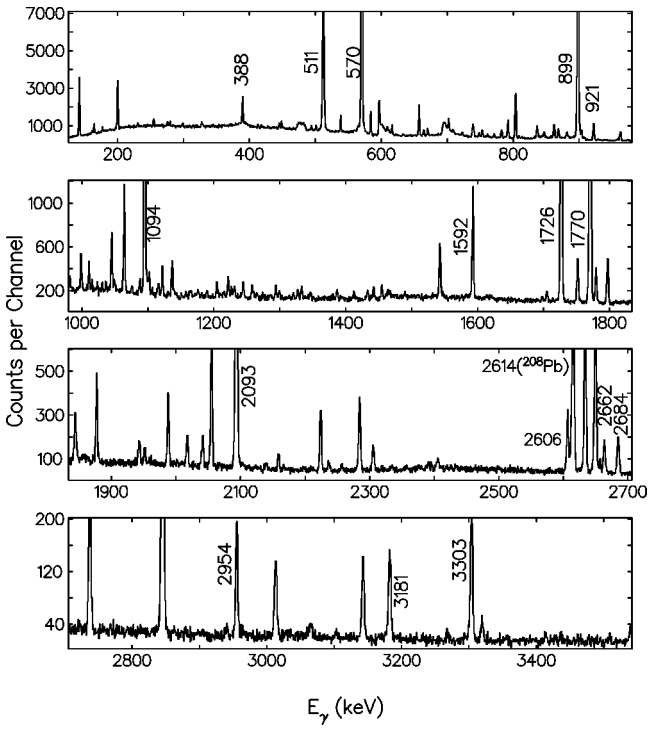

FIG. 1. γ-ray spectrum from the ^{207}Pb$(n,n'\gamma)$ reaction with 4-MeV neutrons. Some of the notable γ rays are labeled with their energies.

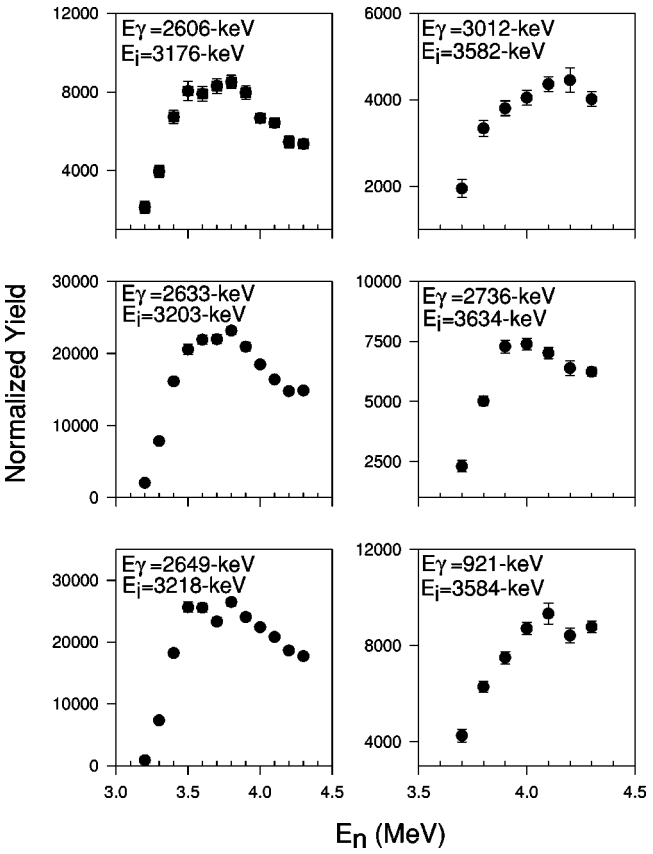

FIG. 2. Excitation functions of some rays from the ^{207}Pb$(n,n'\gamma)$ reaction. γ-ray energies and level energies (thresholds) are indicated.

1.5 cm and a height of 2.1 cm. For the γ-ray singles measurements, including angular distributions and excitation functions, the γ rays were detected with a HPGe detector, with a relative efficiency of 52% and an energy resolution (FWHM) of 2.1 at 1332 keV, located $\simeq$1.1 m from the scattering sample. Time-of-flight gating was employed to reduce extraneous background events, and Compton suppression was achieved using an annular BGO shield. A typical ^{207}Pb spectrum acquired under these conditions is shown in Fig. 1. For all measurements, calibrations for efficiency, energy, and nonlinearity of the system were performed using ^{226}Ra and ^{56}Co sources.

In addition to excitation functions and angular distributions, γ-γ coincidence measurements with 4.6 MeV incident neutrons were performed with four HPGe detectors similar to the one described above [4]. The neutrons were collimated with a Li-loaded pariffin collimator 0.5 m in length, and the scattering sample was located 0.75 m from the neutron production source. The sample-detector distance was approximately 5 cm. Events were recorded whenever two (or more) detectors registered events within a 100 ns window. In the offline analysis of the data, a more stringent requirement of events within $\sim$40 ns and $\pm$20 ns of the beam pulse was placed on the data which were sorted into a $4k\times4k$ matrix.

γ-ray thresholds determined from the excitation functions, measured in 100 keV steps from $E_n=2.5$ to 4.3 MeV, generally allow the identification of the levels from which the γ rays originate. Examples of these excitations functions are shown in Fig. 2. From this γ-ray threshold information and the coincidence relationships, levels and γ rays were placed in the level scheme.

Angular distribution measurements, using 4.0 MeV incident neutrons, included spectra at 12 angles from 39° to 155°. The normalized angular distributions coefficients, a_2 and a_4, can be determined from the Legendre polynomial fits of the angular distribution data according to the equation

$$W(\theta)=I_\gamma[1+a_2P_2(\cos\theta)+a_4P_4(\cos\theta)]. \qquad (1)$$

Comparison of the experimental a_2 and a_4 coefficients (see Table II) with statistical model calculations [5] can be used to limit the spin assignments. Examples of typical angular distributions are shown in Fig. 3.

The observed Doppler shifts of the γ-ray energies as a function of angle provided a means of level lifetime determination. The Doppler-shifted γ-ray energy $E_\gamma(\theta)$ is given by

$$E_\gamma(\theta_\gamma)=E_0[1+\beta F(\tau)\cos\theta_\gamma], \qquad (2)$$

where $E_\gamma(\theta_\gamma)$ is the observed γ-ray energy at an angle θ_γ with respect to the recoil direction (taken to be the direction of the incident neutron), E_0 is the unshifted γ-ray energy, and $\beta=v/c$ with v the recoil velocity. Applying the methodology described by Belgya *et al.* [6], the Doppler-shift attenuation method was used to obtain the lifetimes of the observed levels. Examples of Doppler shifts are presented in Fig. 4, and Tables I and II contain a listings of the level

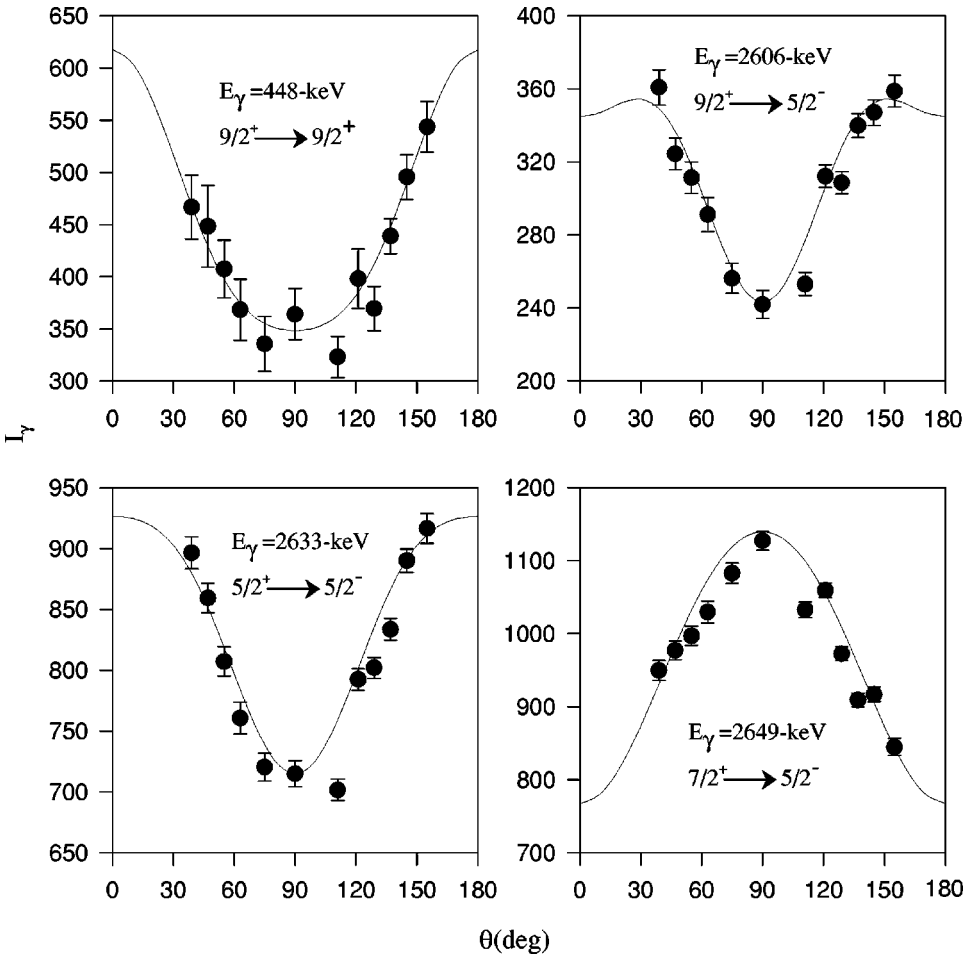

FIG. 3. Angular distributions of some γ-ray transitions from the ^{207}Pb$(n,n'\gamma)$ reaction at 3.4 MeV. The solid lines are theoretically calculated angular distributions using the program CINDY [5].

lifetimes and the $F(\tau)$ values determined. A portion of the lifetime results obtained have been reported previously [3]. The present results extend these earlier measurements.

III. THE ^{207}Pb LEVEL SCHEME

In this ^{207}Pb$(n,n'\gamma)$ study, many of the previously placed levels and transitions [7] were observed along with several new levels and many new γ-ray transitions. By combining the information obtained from the excitation functions, angular distributions, and coincidence measurements, a detailed level scheme was constructed. In Table I, the decay properties of the observed levels in ^{207}Pb are presented. The properties of the levels below 3 MeV are well established and will not be discussed further. It is appropriate, however, that we comment on some of the levels above this energy for which new information is available.

3175.8-keV level. γ rays at 2605.6, 1542.3, 835.7, and 447.8 keV originate from this level. The excitation functions of each of these γ rays exhibit thresholds at approximately 3.2 MeV. Coincidence gates on the 2605- and 447-keV γ rays also support their placements. The 1542-keV γ ray could not be seen in coincidence with other γ rays as it decays to the 1633-keV isomeric level. The angular distribution data limit the spin assignment of this level to 9/2.

3181.7-keV level. The population of this level with the $(n,n'\gamma)$ reaction was questionable in previous work [7]. γ rays of 3181.3, 2612, and 2283.8 keV, with thresholds at 3.2 MeV, depopulate this level. The energy of the 2612-keV γ ray is poorly determined as a result of spectral complications produced by the presence of the strong 2614-keV γ ray of ^{208}Pb. Spin assignments of 1/2 or 3/2 are possible from the angular distribution data.

3202.7-keV level. Like the previous level, the population of this level in previous $(n,n'\gamma)$ measurements was questionable [7]. The 2305.0- and 2633.0-keV γ rays deexcite this level, and the 5/2 assignment is favored by the angular distribution data.

3218.5-keV level. This level, reported first in Ref. [3] decays by a 2648.8-keV γ ray to the first excited state. The γ-ray threshold and the coincidence data support this placement, and a spin of 7/2 is favored by the angular distribution data. Figure 5 shows some coincidence gates used in establishing the placement of γ rays for both 3218- and 3176-keV levels.

3225.7-keV level. The 1592.2-keV γ ray from this level was reported previously [7], but the 2655.3-keV transition to the first excited state was not. The γ-ray thresholds and coincidence measurements support these placements. The shape of the excitation functions and the angular distributions favor a spin 11/2 assignment.

3302.8-keV level. This level and its $1/2^+$ spin-parity had been established; however, only the 3303 transition was observed [8]. Along with the 3303-keV transition, a new 2405-

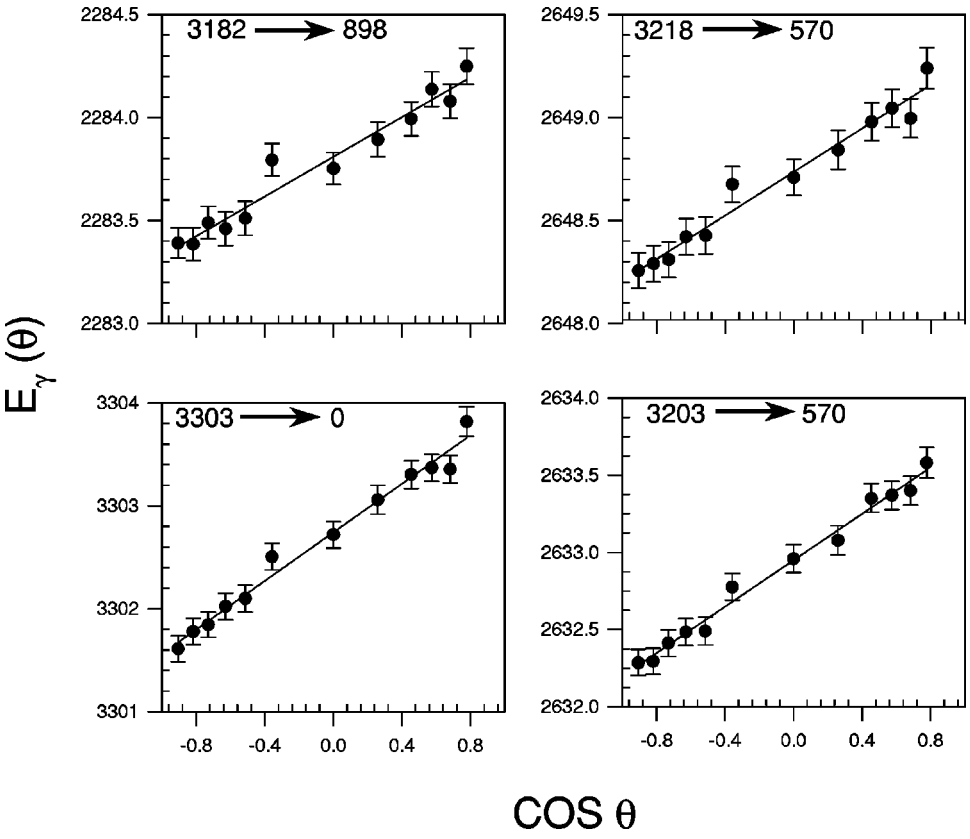

FIG. 4. Measured γ-ray energy as a function of cos θ for selected transitions in ^{207}Pb. $F(\tau)$ values obtained from linear fits to the data and the level lifetimes deduced are given in Tables II and I, respectively.

keV γ-ray branch is also observed.

3384.6-keV level. Recently, the 1044.7-keV γ ray was reported [9] from this state. Along with this γ ray, deexciting transitions of 656.6 and 1751.1 keV are observed.

3414.2- and 3415.4-keV levels. Two levels are observed near this energy, instead of the single level previously reported at 3414 keV [7]. Four γ rays originate from these levels. The 752.9-, 791.7-, and 1075.6-keV γ rays deexcite a level at 3415.43$\pm$0.04 keV, while the 2844.48-keV γ ray is from the 3414.18$\pm$0.08-keV state. Spin arguments also indicate the presence of two levels; the angular distribution of the 2844.5-keV γ ray is consistent with spins of 3/2, 5/2, and 7/2 while that of the 752.9-keV γ ray indicates a higher spin of 9/2 or 11/2.

3476.3-keV level. In addition to the recently reported 1136.4-keV transition [9], new transitions at 748.4 and 1843.1 keV are observed.

3524.1-keV level. This state, along with 861.6- and 2954.2-keV γ rays, was also reported by Radermacher *et al.* [9]. The γ-ray angular distributions are consistent with spin assignments of $5/2^+$ or $7/2^+$.

3582.0- and 3584.1-keV levels. Only one level close to these energies has been previously reported [7]. Six γ rays are observed from these two levels. The measured lifetimes are different for the two levels: 14 fs for the 3582.0-keV level and 160 fs for the 3584.1-keV state. The angular distributions for the three γ rays from the 3582.0-keV level are consistent with low spins (3/2, 5/2, or 7/2), while those of the γ rays from the 3584.1-keV level indicate spins of 9/2 or 11/2.

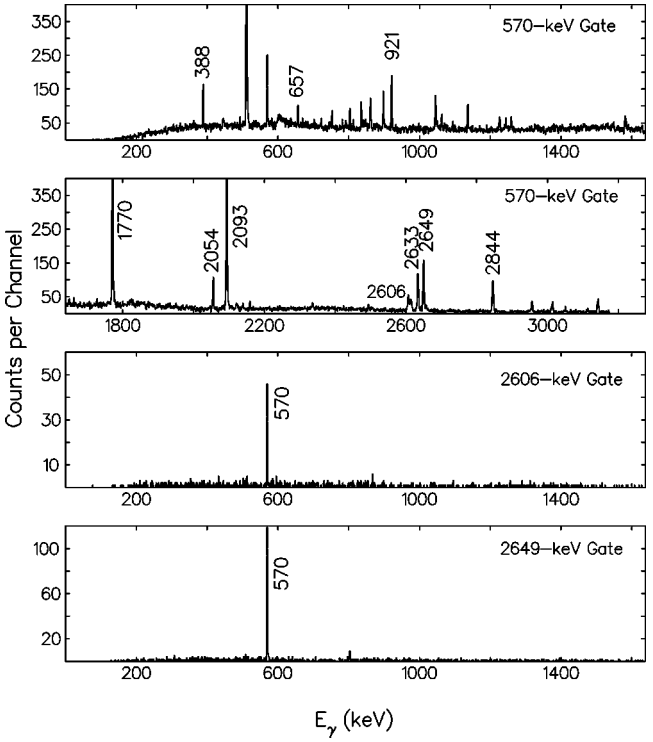

FIG. 5. Coincidence spectra obtained by gating on 570- (top two panels), 2606-, and 2649-keV γ rays of ^{207}Pb.

TABLE I. Summary of level properties in ^{207}Pb.

E_l [keV]	J^π	τ [fs]	E_γ [keV]	E_f	J_f^π	Br
0.0	$1/2^-$					
569.70(2)	$5/2^-$		569.70(1)	0.0	$1/2^-$	1.00
897.92(2)	$3/2^-$		897.92(1)	0.0	$1/2^-$	0.996(1)
			328.15(1)	569.70	$5/2^-$	0.004(1)
1633.43(3)	$13/2^+$		1063.74(1)	569.70	$5/2^-$	1.00
2339.88(3)	$7/2^-$		1770.19(2)	569.70	$5/2^-$	0.98(1)
			1442.13(4)	897.92	$3/2^-$	0.02(1)
2624.11(3)	$5/2^+$		2054.29(2)	569.70	$5/2^-$	0.18(1)
			1726.23(2)	897.92	$3/2^-$	0.82(1)
2662.51(3)	$7/2^+$		2662.25(4)[a]	0.0	$1/2^-$	0.05(1)
			2092.78(2)	569.70	$5/2^-$	0.95(1)
2727.93(3)	$9/2^+$		2158.16(3)[a]	569.72	$5/2^-$	0.02(1)
			1094.77(1)	1633.43	$13/2^+$	0.82(1)
			388.24(2)	2339.88	$7/2^-$	0.16(1)
3175.75(4)[b]	9/2	>580	2605.56(3)[c]	569.72	$5/2^-$	0.34(1)
			1542.32(2)[c]	1633.43	$13/2^+$	0.31(1)
			835.73(2)	2339.88	$7/2^-$	0.21(1)
			447.81(2)[c]	2727.93	$9/2^+$	0.15(1)
3181.74(5)	3/2,1/2	53^{+14}_{-11}	3181.30(4)	0.0	$1/2^-$	0.34(1)
			2612.04[a,d]	569.72	$5/2^-$	
			2283.82(2)	897.92	$3/2^-$	0.66(1)
3202.67(6)	5/2	29^{+9}_{-7}	2632.97(3)	569.72	$5/2^-$	0.870(5)
			2305.03(4)	897.92	$3/2^-$	0.130(5)
3218.46(6)[b]	7/2	56^{+20}_{-14}	2648.75(3)	569.72	$5/2^-$	1.00
3225.65(4)	$11/2^+$	>480	2655.32(7)	569.72	$5/2^-$	0.080(6)
			1592.22(2)	1633.43	$13/2^+$	0.920(6)
3302.77(7)	$1/2^+$	11^{+6}_{-5}	3302.77(4)	0.0	$1/2^-$	0.83(2)
			2405.35(8)	897.92	$3/2^-$	0.17(2)
3384.56(3)	$9/2^+$,$11/2^+$	>410	1751.12(2)[c]	1633.430	$13/2^+$	0.26(1)
			1044.71(2)[a]	2339.88	$7/2^-$	0.20(1)
			656.62(2)[c]	2727.93	$9/2^+$	0.54(1)
3414.18(8)[e]	7/2,5/2,3/2	55^{+28}_{-18}	2844.48(4)[a]	569.72	$5/2^-$	1.00
3415.43(4)[e]	$9/2^-$	230^{+830}_{-120}	1075.63(7)[c]	2339.88	$7/2^-$	0.09(1)
			791.66(2)[a]	2624.11	$5/2^+$	0.61(2)
			752.92(2)[a]	2662.51	$7/2^+$	0.30(1)
3429.90(4)	9/2,11/2	>630	1796.51(2)[c]	1633.43	$13/2^+$	0.61(1)
			701.88(3)[c]	2727.93	$9/2^+$	0.39(1)
3476.31(3)	9/2	>560	1843.09(2)[c]	1633.43	$13/2^+$	0.440(9)
			1136.42(2)[a]	2339.88	$7/2^-$	0.380(7)
			748.40(2)[c]	2727.93	$9/2^+$	0.190(6)
3509.90(4)	$11/2^+$	>300	1876.44(2)[c]	1633.43	$13/2^+$	0.670(6)
			782.00(2)[c]	2727.93	$9/2^+$	0.330(6)
3524.05(4)	7/2,5/2	230^{+240}_{-90}	2954.21(4)[a]	569.70	$5/2^-$	0.41(1)
			861.57(2)[a]	2662.51	$7/2^+$	0.59(1)
3582.05(5)[e]	7/2,5/2,3/2	14 ± 5	3012.32(4)[c]	569.70	$5/2^-$	0.38(1)
			2684.28(3)[c]	897.92	$3/2^-$	0.53(1)
			958.6(1)[c]	2624.11	$7/2^+$	0.09(1)
3584.14(4)[e]	11/2,9/2	160^{+110}_{-50}	1950.79(5)[c]	1633.43	$13/2^+$	0.07(1)
			1244.33(3)[c]	2339.88	$7/2^-$	0.15(1)
			921.66(1)[c]	2662.51	$7/2^+$	0.79(1)
3620.56(5)	$11/2^+$	>350	1987.13(2)[c]	1633.43	$13/2^+$	1.00

TABLE I. (*Continued*.)

E_l [keV]	J^π	τ [fs]	E_γ [keV]	E_f	J_f^π	Br
3634.38(6)	3/2,5/2	140^{+80}_{-40}	2736.46(3)[a]	897.92	$3/2^-$	0.80(1)
			1010.66(3)[a]	2662.51	$7/2^+$	0.20(1)
3650.15(5)		>450	2016.72(3)[c]	1633.43	$13/2^+$	1.00
3673.88(3)	9/2,11/2	>380	2040.45(3)[c]	1633.43	$13/2^+$	1.00
3710.90(7)	$9/2^+$	>170	3141.20(4)[a]	569.70	$5/2^-$	0.61(1)
			1087.58(3)[c]	2624.11	$5/2^+$	0.24(1)
			1048.90(5)[c]	2662.51	$7/2^+$	0.15(1)
3725.32(4)	9/2,7/2	>290	1386.16(6)[c]	2339.88	$7/2^-$	0.10(2)
			1062.82[c,f]	2662.51	$7/2^+$	0.31(3)
			998.20(2)[c]	2727.93	$9/2^+$	0.59(2)
3828.87(5)	$9/2^+$,$11/2^+$	>160	1101.21(2)[c]	2727.93	$9/2^+$	0.37(1)
			444.31(2)[c]	3384.56	$11/2^+$,$9/2^+$	0.64(1)
3869.43(9)	$9/2^+$,$11/2^+$	>150	2236.00(5)[c]	1633.43	$11/2^+$	1.00
3888.71(8)	5/2,7/2	180^{+290}_{-80}	3318.16(5)[a]	569.70	$5/2^-$	0.37(1)
			2255.38(4)[c]	1633.43	$13/2^+$	0.31(1)
			1225.97(3)[c]	2662.51	$7/2^+$	0.33(1)
3903.36(18)		>24	1175.43(10)[c]	2727.93	$9/2^+$	1.00
3927.62			3927.62	0.0	$1/2^-$	1.00
4000.00(5)		110^{+120}_{-50}	1375.89(2)[a]	2624.11	$5/2^+$	1.00
4063.98		>53	1336.12(8)[c]	2727.93	$9/2^+$	1.00
4088.29			3518.59[a]	569.70	$5/2^-$	1.00
4104.04			4104.04	0.0	$1/2^-$	1.00
4127.88			3558.18[c]	569.70	$5/2^-$	1.00
4141.05			4141.05	0.0	$1/2^-$	1.00
4192.3			3622.6[c]	569.70	$5/2^-$	1.00

[a]This transition was observed initially by Radermacher *et al.* [9].

[b]Level reported in Ref. [3] or in the present work, for the first time.

[c]Transition reported for the first time.

[d]Energy from level-energy differences; intensity could not obtained due to spectral complications with the strong 2614-keV γ ray of ^{208}Pb.

[e]See text.

[f]Energy from level-energy differences; intensity not exact due to the presence of 1063.7-keV γ ray from the 1633.4-keV isomer of ^{207}Pb.

IV. RESULTS AND DISCUSSION

The states in ^{207}Pb below 2.5 MeV have been described as single-hole states in the doubly magic ^{208}Pb core [10]. The properties of these levels are generally well established and are not discussed further.

A. Weak coupling in ^{207}Pb

The coupling of the $h_{9/2}$ (or $p_{1/2}^{-1}$) ground states of ^{209}Bi (or ^{207}Pb) with the 3^- core excitation, the octupole phonon at 2614-keV in ^{208}Pb, is expected to result in a multiplet of states at an energy of ~2600 keV. A septuplet of states in ^{209}Bi, with spins from $3/2^+$ to $15/2^+$, has long been known and is frequently used as a textbook example illustrating particle-vibration coupling [11,12]. Although the $15/2^+$ state is somewhat separated from the other members of the septuplet, this deviation can be explained by considering the mixed configuration of this state [13,14]. Weak coupling is also observed in ^{207}Pb, where a neutron hole, instead of a proton particle as in ^{209}Bi, is coupled to the 3^- octupole core excitation. The $3^- \otimes p_{1/2}^{-1}$ coupling is expected to give rise to a doublet at ~2600 keV, and states at 2624 ($5/2^+$) and 2662 ($7/2^+$) keV have been characterized [15,16] as these excitations. The enhanced $E3$ ground-state transition from the 2662-keV state, initially observed by Radermacher *et al.* [9], lends additional support to the weak-coupling interpretation of these states.

A sextuplet of states ($1/2^+$ to $11/2^+$) at ~3200 keV from the $3^- \otimes f_{5/2}^{-1}$ coupling [15] is anticipated in ^{207}Pb. In this energy region, levels at 3182-, 3203-, 3226-, and 3303-keV had been reported [7,9]. We have observed additional levels at 3176- and 3218-keV in this study, bringing the total to six levels in this energy region with the spins consistent with the $3^- \otimes f_{5/2}^{-1}$ coupling picture.

The presence of these six isolated states at energies near 3.2 MeV, with a small energy splitting, indicates that this is a clear example of weak coupling. The observation of new $E3$ transitions from this multiplet also supports the idea that it is indeed a $3^- \otimes f_{5/2}^{-1}$ coupling. The separation of the $1/2^+$ member at 3303-keV from the other members of the sextu-

TABLE II. Angular distribution coefficients and the attenuation coefficients from the ^{207}Pb$(n,n'\gamma)$ reaction.

E_γ (keV)	a_2	a_4	$F(\tau)_{\rm exp}$	E_γ (keV)	a_2	a_4	$F(\tau)_{\rm exp}$
388.24	−0.18(3)	0.02(4)	0.01(36)	1726.23	−0.15(3)	−0.01(4)	0.23(6)
444.31	0.42(4)	0.04(6)	0.07(35)	1751.12	0.24(4)	−0.04(5)	0.01(8)
447.81	0.39(6)	0.10(8)	0.27(37)	1770.19	−0.08(3)	−0.01(4)	0.35(6)
596.70	0.18(3)	−0.03(4)	0.0(21)	1796.51	−0.74(3)	0.06(5)	
656.62	0.38(4)	−0.04(5)	0.07(17)	1843.09	0.13(7)	−0.22(10)	0.01(9)
701.88	0.54(9)	0.08(12)	0.10(29)	1876.44	0.48(4)	0.02(6)	0.06(8)
748.40	−0.11(5)	0.06(7)		1950.79	0.24(10)	0.18(14)	0.14(16)
752.92	0.43(5)	−0.02(7)	0.15(17)	1987.13	−0.05(3)	−0.02(5)	0.04(8)
782.00	−0.80(4)	−0.07(6)	0.08(19)	2016.72	0.24(4)	0.05(5)	
791.66	−0.35(11)	−0.50(17)	0.10(20)	2040.45	0.29(4)	−0.01(6)	0.01(10)
835.73	−0.13(7)	0.12(9)	0.03(18)	2054.29	0.22(4)	−0.05(5)	0.24(7)
861.57	0.24(3)	0.01(4)	0.09(14)	2092.78	−0.17(3)	−0.03(5)	0.07(7)
897.92	−0.05(3)	−0.001(4)	0.17(10)	2158.16	0.11(10)	−0.05(15)	0.05(11)
921.61	−0.14(3)	−0.03(5)	0.22(11)	2236.00	0.52(7)	0.0(1)	0.10(14)
958.60	0.68(24)	0.06(35)	1.10(66)	2255.38	0.53(7)	−0.01(10)	
998.20	0.35(3)	−0.01(5)	0.11(12)	2283.82	0.05(5)	−0.01(7)	0.47(8)
1010.66	0.05(13)	−0.32(20)	0.26(18)	2305.03	−0.07(4)	−0.03(6)	0.52(13)
1044.71	−0.17(4)	−0.01(5)	0.08(11)	2405.35	−0.17(9)	0.01(13)	0.84(25)
1048.90	0.49(16)	0.02(23)		2605.56	0.28(4)	−0.14(6)	0.02(8)
1062.82	−0.02(3)	−0.04(5)	0.03(10)	2612.04[a]			
1075.63	0.35(20)	0.33(27)	0.54(42)	2632.97	0.19(3)	−0.04(5)	0.64(7)
1087.58	−0.14(5)	0.001(70)	0.08(17)	2648.75	−0.2(3)	−0.02(4)	0.45(7)
1094.77	0.18(3)	−0.02(5)	0.02(8)	2655.32	0.86(15)	0.07(20)	
1101.21	0.20(5)	−0.07(8)	0.01(12)	2662.25	0.59(6)	0.17(8)	0.05(11)
1136.42	−0.2(3)	−0.04(5)	0.04(10)	2684.28	−0.18(2)	−0.06(33)	0.76(9)
1175.43	0.32(11)	0.16(14)	0.07(59)	2736.46	−0.20(3)	−0.06(5)	0.24(8)
1225.97	0.33(7)	−0.02(10)	0.21(19)	2844.48	0.02(4)	−0.07(6)	0.45(1)
1244.33	−0.21(9)	0.15(12)	0.30(16)	2954.21	−0.17(4)	0.07(5)	0.19(9)
1336.12	0.13(12)	0.06(17)	0.06(40)	3012.32	0.17(5)	−0.03(7)	0.77(9)
1375.89	0.28(4)	0.02(6)	0.29(12)	3141.20	−0.24(3)	−0.02(5)	0.09(9)
1386.16	−0.59(19)	0.04(27)	0.05(37)	3181.30	−0.07(5)	0.08(6)	0.46(9)
1442.13	0.35(8)	−0.05(11)	0.27(18)	3302.77	−0.06(3)	−0.4(4)	0.80(9)
1542.32	0.21(2)	−0.03(4)		3318.16	−0.30(6)	0.10(80)	0.20(12)
1592.22	−0.28(3)	−0.01(4)	0.03(7)				

[a]Transition not resolved from 2614.5-keV ^{208}Pb γ ray.

plet has been attributed to the fact that it contains a significant (a few percent) fragment of the deep-lying $3s_{1/2}$ hole state [17]. This contribution is consistent with its strong population in nuclear resonance fluorescence and the fast $E1$ decay to the ground state [18]. Figure 6 shows the observed transitions from the decay of the proposed $3^-\otimes f_{5/2}^{-1}$ sextuplet in ^{207}Pb. The configurations of the lower-lying excitations are also indicated. While additional weak-coupling multiplets in ^{207}Pb are expected, their identification becomes more difficult as the level density increases rapidly in the region near 3.5 MeV.

B. $E1$ transition strengths and the ^{208}Pb two-phonon quartet

Recently, the lowest-spin member of the two-phonon octupole quartet in ^{208}Pb was reported by observing an $E3$-$E3$ cascade of transitions from the 0^+ state at 5241-keV [2]. As noted earlier, $E1$ transitions are expected to dominate the decays of other two-phonon octupole excitations, making the observation of $E3$ transitions unlikely. By comparing the $E1$ transition rates from the particle(hole)-octupole coupled states in ^{209}Bi (and ^{207}Pb), which are expected to be similar to the $E1$ transitions from the destruction of the two-phonon quartet, Yeh *et al.* [3] proposed candidates for the 2^+ and 4^+ members of the two-phonon octupole in ^{208}Pb. A summary of the $E1$ transitions from the octupole-coupled states in ^{207}Pb is presented in Table III.

$E1$ decays involving only the destruction of the octupole phonon are not possible from the $3^-\otimes p_{1/2}^{-1}$ doublet; however, the fast 1726-keV $E1$ transition from the 2624-keV $5/2^+$ state to the 898-keV $3/2^-$ $(\nu p_{3/2}^{-1})$ state occurs. The enhanced rate of this decay has been attributed to admixtures in the wave functions of the initial and final states [19].

In principle, the $3/2^+$, $5/2^+$, and $7/2^+$ states of the $3^-\otimes f_{5/2}^{-1}$ sextuplet might be expected to decay to the 570-

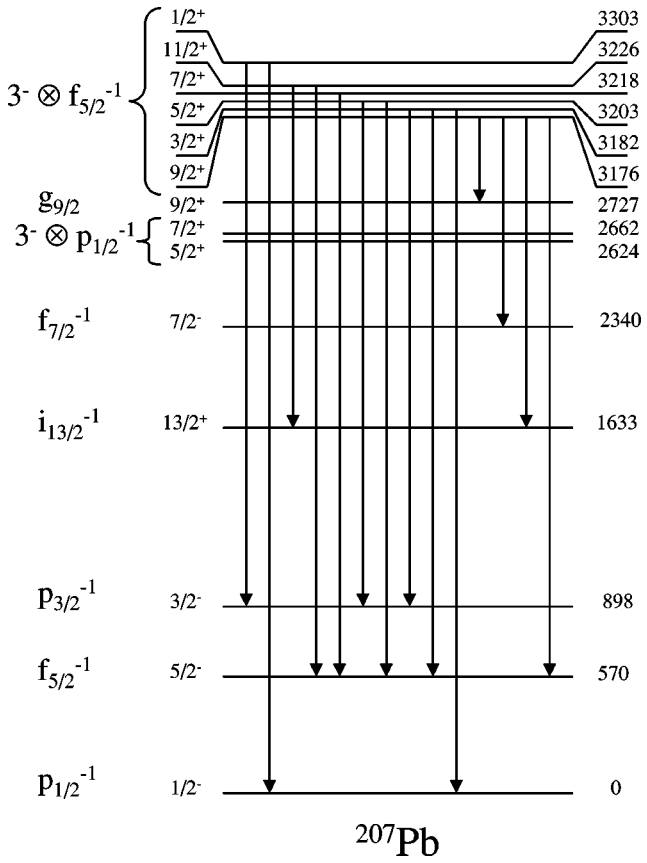

FIG. 6. Low-lying states of ^{207}Pb with their assigned configurations.

keV $f_{5/2}^{-1}$ state by $E1$ transitions that involve the destruction of the octupole phonon. Because of spectral complications, the transition rates of only the latter two decays could be determined, and they are among the fastest $E1$ transitions in ^{207}Pb. However, the fastest $E1$ transition from the sextuplet, and the fastest $E1$ transitions we observe in ^{207}Pb, is the ground-state decay of the 3303-keV $1/2^+$ state. As noted earlier, this fast transition has been attributed to the presence of a few percent of the total $3s_{1/2}^{-1}$ strength in the initial state [17], thus the contribution of an ''allowed'' $s_{1/2} \rightarrow p_{1/2}$ transition yields the large $B(E1)$ value.

TABLE III. $E1$ transitions from the hole-vibration coupled states in ^{207}Pb.

E_i [keV]	E_γ [keV]	J_i^π	J_f^π	τ [fs]	$B(E1)$ [W.u.]
2624	2054	$5/2^+$	$5/2^-$	130 ± 50[a]	$4.3\pm1.4\times10^{-5}$
2624	1726	$5/2^+$	$3/2^-$	130 ± 50[a]	$3.4\pm1.1\times10^{-4}$
2662	2093	$7/2^+$	$5/2^-$	950 ± 200[a]	$3.0\pm0.6\times10^{-5}$
3176	836	$9/2^+$	$7/2^-$	>600	$<1.7\times10^{-4}$
3182	3181	$3/2^+,1/2^+$	$1/2^-$	53 ± 13	$5.5\pm1.4\times10^{-5}$
3182	2284	$3/2^+,1/2^+$	$3/2^-$	53 ± 13	$2.9\pm0.7\times10^{-4}$
3203	2633	$5/2^+$	$5/2^-$	29 ± 8	$4.5\pm1.2\times10^{-4}$
3218	2649	$7/2^+$	$5/2^-$	56 ± 17	$2.6\pm0.8\times10^{-4}$
3302	3302	$1/2^+$	$1/2^-$	11 ± 6	$5.7\pm3.1\times10^{-4}$
3302	2405	$1/2^+$	$3/2^-$	11 ± 6	$1.4\pm0.8\times10^{-4}$

[a]From Ref. [19].

C. $E3$ transitions

Transition probabilities for exciting the individual states resulting from the weak coupling between the neutron hole and the octupole phonon in ^{208}Pb can be approximated by [12]

$$B[E3,n_\lambda=0,\ j\rightarrow(n_\lambda=1,j)I] = \frac{(2I+1)}{(2l+1)(2j+1)}B(E3,n_\lambda=0\rightarrow n_\lambda=1). \tag{3}$$

From this equation, $E3$ strengths for the observed transitions in ^{207}Pb can be estimated using the accepted value of 34.0 $\pm$0.5 W.u. for the $B(E3)$ of the 2614-keV transition in ^{208}Pb [20]. With the reported lifetime of 0.95 ± 0.20 ps for the 2662-keV level [19] and the branching ratio from our work, a $B(E3)$ value of 38 ± 8 W.u. is obtained for the $7/2^+ \rightarrow 1/2^-$ transition, while 34 W.u. is obtained from the above equation.

By performing the same kind of calculations for the other observed $E3$ transitions for which definite experimental lifetimes could not be obtained, we can obtain lifetime estimates. For the 2606- and 2655-keV (presumably $E3$) transitions, the calculated level lifetimes are 5.8 and 1.2 ps, respectively. These values are consistent with the lifetime limits obtained for the 3176- and 3226-keV states.

D. Particle-core model calculations

In order to examine the accuracy of the description provided by the macroscopic phonon picture, we have studied the properties of the low-lying levels in ^{207}Pb in the framework of the particle-core coupling model (PCM) [21–24]. The model space for the odd-mass nucleus consists of single-particle states coupled to collective quadrupole and octupole vibrational excitations of the underlying even-even core. In addition to the ''natural'' configuration space consisting of collective excitations in ^{208}Pb coupled to neutron-hole excitations, an additional subspace, which accounts for neutron one-particle, two-hole ($1p$-$2h$) excitations with the odd particle belonging to the shell $N\geqslant126$ have been included. This latter part of the model space can be approximated to a good degree by particle excitations ($N\geqslant126$) coupled to the collective excitations of ^{206}Pb. For each subspace, the Hamiltonian includes a single-particle, a collective and an interaction part, and can be written as

$$\hat{H}=\sum_j \hat{h}_{\rm sp}(j)+\sum_{\lambda=2,3}\hat{H}_{\rm coll}(\lambda)+\hat{H}_{\rm PVC}, \tag{4}$$

with

$$\hat{h}_{\rm sp}(j)=\epsilon_j\, a_j^\dagger\cdot\tilde{a}_j, \quad \hat{H}_{\rm coll}(\lambda)=\left(\hat{n}_\lambda+\frac{2\lambda+1}{2}\right)\hbar\omega_\lambda,$$

and

$$\hat{H}_{\mathrm{PVC}} = -\sum_{\lambda=2,3} \xi_\lambda \hbar\omega_\lambda \left(\frac{\pi}{2\lambda+1}\right)^{1/2} \frac{r^\lambda}{\langle r^\lambda\rangle} \times \sum_{\mu=-\lambda}^{\lambda} [b^\dagger_{\lambda\mu} + (-)^\mu b_{\lambda-\mu}] Y^*_{\lambda\mu}(\hat{r}), \qquad (5)$$

where ϵ_j is the single-particle energy of a given orbital (nlj), ξ_λ gives the strength of the particle-vibration coupling of multipole λ, $\hbar\omega_\lambda$ provides the energy of the vibrational 2^λ pole phonon, $\langle r^\lambda\rangle$ is the mean value of the radial integral for the orbitals in the major shell, $\hat{n}_\lambda$ is the boson number operator, and $a^\dagger_j$, $\tilde{a}_j$ and $b^\dagger_{\lambda\mu}$, $b_{\lambda-\mu}$ are the creation and annihilation operators for the fermionic (single-particle) and bosonic (collective phonons) excitations, respectively.

All the neutron-hole orbitals ($3p^{-1}_{1/2}$, $2f^{-1}_{5/2}$, $3p^{-1}_{3/2}$, $1i^{-1}_{13/2}$, $2f^{-1}_{7/2}$, and $1h^{-1}_{9/2}$) in the shell $N=82$–126 are considered in the ''^{208}Pb subspace,'' as well as the neutron-particle orbitals ($2g_{9/2}$, $1i_{11/2}$, $3d_{5/2}$, $1j_{15/2}$, $4s_{1/2}$, $2g_{7/2}$, and $3d_{3/2}$) above $N=126$ in the ''^{206}Pb subspace.'' The coupling of the two subspaces is treated in the manner described in Ref. [25].

The dimensionless particle-vibration coupling strengths of multipole λ are related to the experimental $B(E\lambda)$ values by

$$\xi_\lambda = \frac{\beta_\lambda}{\sqrt{\pi}} \frac{\langle k_\lambda(r)\rangle}{\hbar\omega_\lambda}, \quad \beta_\lambda = \frac{[B(E\lambda;0^+\rightarrow\lambda)]^{1/2}}{3/4\pi ZeR_0^\lambda}. \qquad (6)$$

The average value of the radial coupling factor at the surface of the nucleus $\langle k_\lambda(r)\rangle$, was estimated to be 40–50 MeV for medium heavy and heavy nuclei [26], which results in a quite broad interval of possible ξ_λ values. We have therefore fixed the best values of the particle-vibration coupling strengths from a careful comparison of the properties (energies and spectroscopic factors) of the calculated and experimental levels of all four odd-mass nuclei adjacent to ^{208}Pb. The quadrupole coupling strength was found to correspond to weak coupling ($\xi_2=0.35$), and the octupole strength to intermediate coupling ($\xi_3=1.15$).

The collective configurations taken into account in the calculations include up to three quadrupole phonons, two octupole phonons, and one quadrupole-one octupole phonon state. Anharmonicities are considered by allowing for nonzero mass quadrupole moments of the quadrupole and octupole phonons [24,27]. This approach leads to quadrupole-quadrupole diagonal terms which remove the degeneracy in the multiphonon spectrum as well as in the particle(hole)-phonon multiplets. The quadrupole moments of the single-particle orbitals are calculated using the wave functions obtained with the Woods-Saxon potential with the parameters of Ref. [28]. The *mass* quadrupole moments of the phonons, deduced from comparison of the properties of the calculated and experimental members of phonon $\otimes$ particle multiplets are found to be $Q(2^+)=-20$ fm^2 for the quadrupole and $Q(3^-)=-25$ fm^2 for the octupole phonon. Because of the small magnitude of the coupling constant involved in the diagonal quadrupole-quadrupole Hamiltonian, $\kappa_2=-0.4568\ 10^{-3}$ MeV fm^{-4} [26], and also of the quadrupole moments involved, the effects of the quadrupole-quadrupole splitting within the hole-phonon or phonon-phonon multiplets are reduced and are typically of the order of 100 keV.

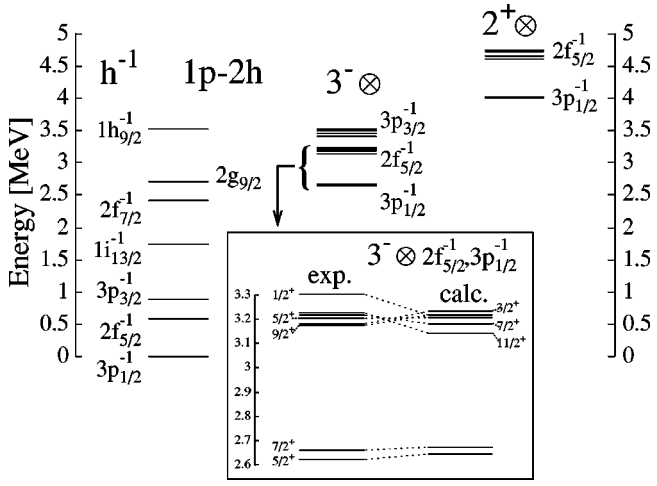

FIG. 7. Selected states with dominant $1h$, $1p$-$2h$ (left side), and hole-phonon configuration (middle and right side). An energy cutoff of 3.5 MeV was chosen for the $1h$, $1p$-$2h$, and hole-octupole phonon states, and of 5 MeV for the quadrupole-coupled states. The dominant configuration of the states is indicated. In the blown-up region, the $3^-\otimes 2f^{-1}_{5/2}$ and $3^-\otimes 3p^{-1}_{1/2}$ multiplets are shown in greater detail and compared to the experimental data.

No microscopic structure of the phonons is taken into account, and, consequently, the effects of the Pauli principle on the properties of states of the type phonon $\otimes$ hole are not described.

The results of the PCM calculations confirm indeed the weak-coupling expectations. The $3^-\otimes f^{-1}_{5/2}$ and $3^-\otimes p^{-1}_{1/2}$ multiplets are predicted to be quite pure. For all the spin values involved, the octupole $\otimes$ hole configuration amounts to 90% or more of the wave function. We mention that the deep-lying hole state $3s^{-1}_{1/2}$ is not included in the model space. Instead, the $1/2^+$ member of the $3^-\otimes f^{-1}_{5/2}$ multiplet, at 3303 keV, is predicted to contain a small component (around 4%) of the $4s_{1/2}$ single-particle configuration, which may contribute to the observed fast $E1$ transition to the ground state.

We present in Fig. 7 selected results of the calculation. The states with dominant neutron-hole component are shown on the left side of the figure, as well as the lowest $9/2^+$ state with neutron $2g_{9/2}$ $1p-2h$ structure. The higher-lying $1p-2h$ configurations generally show more fragmentation. In the middle part of the figure, the hole-octupole phonon multiplets up to 3.5 MeV are presented. The $3^-\otimes 3p^{-1}_{1/2}$, $3^-\otimes 2f^{-1}_{5/2}$, and $3^-\otimes 3p^{-1}_{3/2}$ multiplets are included in this energy range and are characteristic of a weak-coupling picture. The lowest two hole-quadrupole phonon multiplets $2^+\otimes 3p^{-1}_{1/2}$ and $2^+\otimes 2f^{-1}_{5/2}$, are finally presented on the right side. The two hole-octupole multiplets of interest for our study are shown in more detail in the expanded portion, and are compared to the experimental data. While there are some

TABLE IV. Calculated and experimental reduced $E1$ transition probabilities from the hole-vibration coupled states in ^{207}Pb. Only the core contribution to the transition probabilities is taken into account in the calculated values.

J_i^π	$E_i^{\rm exp}$ [keV]	$E_i^{\rm calc}$ [keV]	Struct.	J_f^π	$E_f^{\rm exp}$ [keV]	$E_f^{\rm calc}$ [keV]	Struct.	$E_\gamma^{\rm exp}$ [keV]	$B(E1)_{\rm exp}$ [W.u.]	$B(E1)_{\rm calc}$ [W.u.]
$5/2_1^+$	2624	2646	$3^-\times p_{1/2}^{-1}$	$5/2_1^-$	570	580	$f_{5/2}^{-1}$	2054	$4.3\pm1.4\times10^{-5}$	$0.54^{+0.29}_{-0.24}\times10^{-6}$
$5/2_1^+$	2624	2646	$3^-\times p_{1/2}^{-1}$	$3/2_1^-$	898	888	$p_{3/2}^{-1}$	1726	$3.4\pm1.1\times10^{-4}$	$0.95^{+0.49}_{-0.42}\times10^{-5}$
$7/2_1^+$	2662	2673	$3^-\times p_{1/2}^{-1}$	$5/2_1^-$	570	580	$f_{5/2}^{-1}$	2093	$3.0\pm0.6\times10^{-5}$	$0.84^{+0.44}_{-0.37}\times10^{-5}$
$3/2_1^+$	3182	3234	$3^-\times f_{5/2}^{-1}$	$1/2_1^-$	0	0	$p_{1/2}^{-1}$	3181	$5.5\pm1.4\times10^{-5}$	$0.85^{+0.44}_{-0.38}\times10^{-5}$
$3/2_1^+$	3182	3234	$3^-\times f_{5/2}^{-1}$	$3/2_1^-$	898	888	$p_{3/2}^{-1}$	2284	$2.9\pm0.7\times10^{-4}$	$2.01^{+1.05}_{-0.89}\times10^{-6}$
$5/2_2^+$	3203	3208	$3^-\times f_{5/2}^{-1}$	$5/2_1^-$	570	580	$f_{5/2}^{-1}$	2633	$4.5\pm1.2\times10^{-4}$	$0.52^{+0.27}_{-0.23}\times10^{-5}$
$7/2_2^+$	3218	3183	$3^-\times f_{5/2}^{-1}$	$5/2_1^-$	570	580	$f_{5/2}^{-1}$	2649	$2.6\pm0.8\times10^{-4}$	$0.73^{+0.38}_{-0.33}\times10^{-5}$
$1/2_1^+$	3302	3217	$3^-\times f_{5/2}^{-1}$	$1/2_1^-$	0	0	$p_{1/2}^{-1}$	3302	$5.7\pm3.1\times10^{-4}$	$2.1^{+1.1}_{-0.9}\times10^{-5}$
$1/2_1^+$	3302	3217	$3^-\times f_{5/2}^{-1}$	$3/2_1^-$	898	888	$p_{3/2}^{-1}$	2405	$1.4\pm0.8\times10^{-4}$	$0.76^{+0.40}_{-0.34}\times10^{-6}$

discrepancies between the calculated and experimental levels, concerning the ordering of the members of the $3^-\otimes 2f_{5/2}^{-1}$ multiplet, the energy differences generally stay well within 100 keV. The deviation of the calculated multiplet from the ''parabolic rule'' obtained for the diagonal quadrupole-quadrupole interaction (see, for example, the discussion of Ref. [22] for proton-neutron multiplets, which also applies for particle-phonon multiplets) is due to the (different for each J) interaction of most of the multiplet members with $1p$-$2h$ configurations with the corresponding spin and parity.

We further studied within the model the fast $E1$ transitions observed experimentally. There are two major types of contributions to the transition amplitudes—from the core and from the single-particle $E1$ transitions. The $E1$ operator can be written as

$$T(E1)=T_{\rm coll}(E1)+T_{\rm sp}(E1). \tag{7}$$

We briefly discuss the separate terms in the operator.

The magnitude of the core contribution can be inferred from the value of the rather fast $E1$ transition connecting the first 2^+ state and the first 3^- state in ^{208}Pb. The collective $E1$ transition operator acting in the quadrupole and octupole phonon space can be written as

$$T_{\rm coll}(E1)_{1\mu}={\rm const}(b_2b_3^\dagger+b_3b_2^\dagger+b_2^\dagger b_3^\dagger+b_3b_2)_{1\mu}, \tag{8}$$

where the constant in the above expression can be deduced by requiring that the collective operator, acting between the 2_1^+ and the 3_1^- states of the core, should reproduce the experimental $B(E1)$ value of $(4\pm2)\times10^{-4}$ W.u. [30]. From this requirement one can deduce only the absolute value of the constant; the sign was chosen to be positive, because the results obtained in this case were much more consistent with the experiment. The collective $E1$ operator connects components in the wave functions of the initial and final states of the type $3^-\otimes j\rightleftharpoons 2^+\otimes j$ (where j stands for either a neutron-hole or a neutron-particle orbital) and of the type $(2^+\otimes3^-)1^-\otimes j\rightleftharpoons 0^+_{\rm g.s.}\otimes j$.

The single-particle operator is written as

$$T_{\rm sp}(E1)_{1\mu}=e_{\rm eff}\ rY_{1\mu}, \tag{9}$$

where the effective charge $e_{\rm eff}$ is a positive quantity and depends on the orbitals involved. In the configuration space built from collective excitations in ^{208}Pb and neutron-hole excitations, the single-particle $E1$ operator cannot connect any of the single-particle orbitals considered. The same is valid in the configuration space built from collective excitations in ^{206}Pb and neutron-particle excitations. Nevertheless, the $E1$ transitions between neutron-hole states and neutron-particle states are allowed. Even very small components of neutron-particle configurations in the wave functions of the (for example) initial states lead to components in the $E1$ transition probability to final states of predominantly neutron-hole structure which are equally large or larger than the core contribution.

To illustrate the above considerations, we consider a simplified structure of the $5/2_1^-$ state and the different $E1$ transition amplitudes leading to different final configurations.

$$\begin{array}{ccccc} \alpha|0^+\otimes f_{5/2}^{-1}\rangle & & +\beta|2^+\otimes f_{5/2}^{-1}\rangle & & +\cdots, \\ \Downarrow \text{ core } E1 & & \Downarrow \text{ core } E1 & & \\ |(2^+\otimes3^-)1^-\otimes f_{5/2}^{-1}\rangle & & |3^-\otimes f_{5/2}^{-1}\rangle & & \cdots. \end{array}$$

Some other possible contributions come from single-particle $E1$ transitions between hole- and particle-orbitals belonging to the two different shells, as shown in the diagram below.

$$\begin{array}{ccccc} & & \alpha|0^+\otimes 2f_{5/2}^{-1}\rangle & & \cdots \\ & +\text{s.p.}E1\swarrow & \downarrow & & \searrow\text{s.p.}E1, \\ |0^+(2)\otimes3d_{5/2}\rangle, & & |0^+(2)\otimes2g_{7/2}\rangle, & & |0^+(2)\otimes3d_{3/2}\rangle. \end{array}$$

In the diagram above, $0^+(2)$ stands for the ground state of ^{206}Pb (the second core), which can be written as a superposition of neutron-hole pairs occupying the $2f_{7/2}^{-1}$, $2f_{5/2}^{-1}$, $3p_{3/2}^{-1}$, $3p_{1/2}^{-1}$, $1h_{9/2}^{-1}$, and $1i_{13/2}^{-1}$ orbitals. The $0^+(2)$

TABLE V. Energies, spectroscopic factors and $E1$ transitions from the hole-vibration coupled states in ^{207}Pb. Both the core and single-particle contributions have been taken into account. The effective charge used for all the single-particle $E1$ transitions is $e_{\rm eff}=0.08$.

J_i^π	$E_i^{\rm exp}$ [keV]	$E_i^{\rm calc}$ [keV]	$S^{\rm exp}$	$S^{\rm calc}$	J_f^π	$E_f^{\rm exp}$ [keV]	$E_f^{\rm calc}$ [keV]	$S^{\rm exp}$	$S^{\rm calc}$	$E_\gamma^{\rm exp}$ [keV]	$B(E1)_{\rm exp}$ [W.u.]	$B(E1)_{\rm calc}$ [W.u.]
$5/2_1^+$	2624	2646	0.006	0.05	$5/2^-$	570	585	0.6	0.97	2054	$4.3\pm1.4\times10^{-5}$	1.1×10^{-5}
$5/2_1^+$	2624	2646	0.006	0.05	$3/2_1^-$	898	880	0.88	0.96	1726	$3.4\pm1.1\times10^{-4}$	5.7×10^{-4}
$7/2_1^+$	2662	2673	0.031	0.02	$5/2_1^-$	570	585	0.6	0.97	2093	$3.0\pm0.6\times10^{-5}$	3.5×10^{-4}
$3/2_1^+$	3182	3234	—	0.01	$1/2_1^-$	0	0	0.9	0.97	3181	$5.5\pm1.4\times10^{-5}$	1.4×10^{-4}
$3/2_1^+$	3182	3234	—	0.01	$3/2_1^-$	898	880	0.88	0.96	2284	$2.9\pm0.7\times10^{-4}$	2.6×10^{-5}
$5/2_2^+$	3203	3208	[a]	0.02	$5/2_1^-$	570	585	0.6	0.97	2633	$4.5\pm1.2\times10^{-4}$	3.3×10^{-7}
$7/2_2^+$	3218	3183	—	0.008	$5/2_1^-$	570	585	0.6	0.97	2649	$2.6\pm0.8\times10^{-4}$	1.5×10^{-4}
$1/2_1^+$	3302	3217	[a]	0.04	$1/2_1^-$	0	0	0.9	0.97	3302	$5.7\pm3.1\times10^{-4}$	0.9×10^{-4}
$1/2_1^+$	3302	3217	[a]	0.04	$3/2_1^-$	898	880	0.88	0.96	2405	$1.4\pm0.8\times10^{-4}$	4.5×10^{-4}

[a]Seen in the (d,p) reaction; no spectroscopic factor reported.

state can be then written as $\Sigma_i\alpha_i(a_ia_i)_{0^+}|^{208}\mathrm{Pb}\ (\mathrm{g.s.})\rangle$, where i labels the neutron-hole orbitals. The different single-particle transitions described in the last diagram lead to different states (different J values), while the core transitions (first diagram) can lead to different components in the wave-function of the same state.

The rather fast $E1$ transitions observed experimentally connect states of primarily octupole $\otimes$ hole structure with states of main neutron-hole structure. We present in Table IV the calculated $B(E1)$ values for these transitions, taking into account in a first step only the core contribution to the transition probabilities. The experimental values are also shown, together with the main component in the wave functions of the initial and final states. The errors in the $B(E1)$ values are due to the experimental uncertainty for the value of the $B(E1;2_1^+\rightarrow3_1^-)$ in ^{208}Pb.

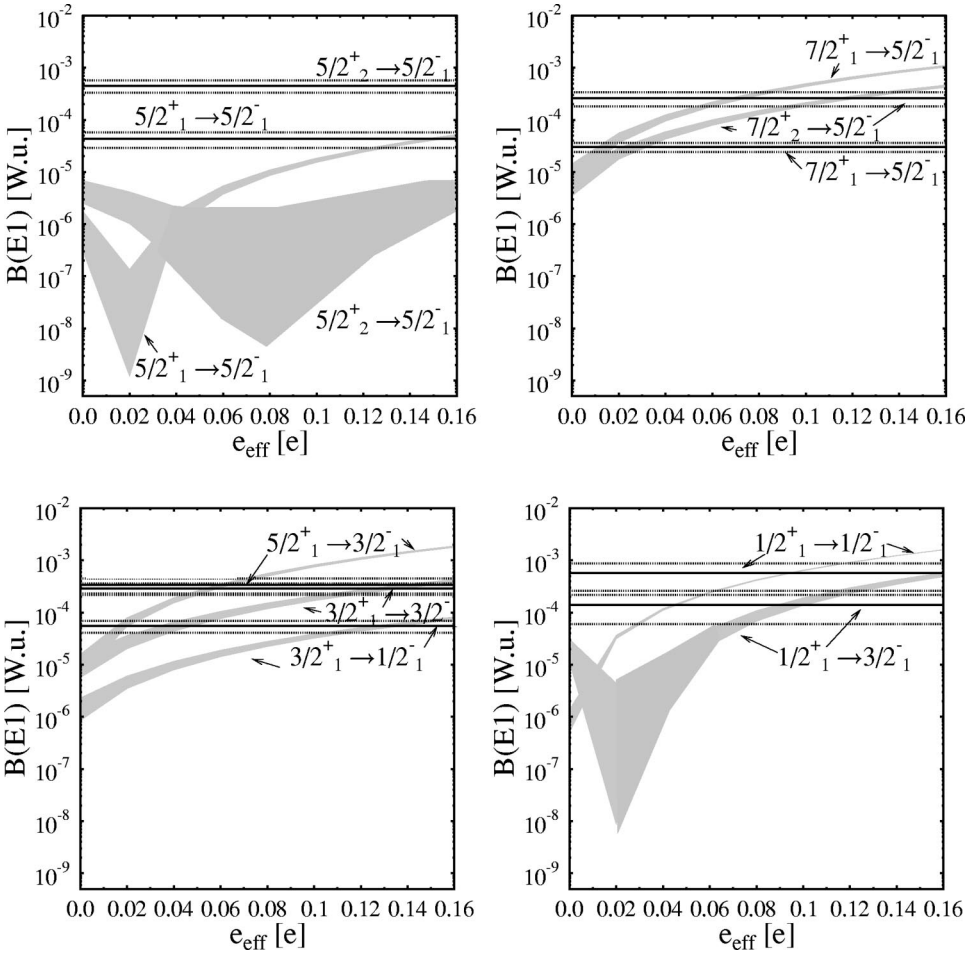

FIG. 8. Dependence of the calculated $B(E1)$ values (shaded areas) on the effective charge. The experimental values are plotted with lines.

It is rather clear that the transition probabilities are underestimated and the core contribution alone is not able to describe the experimental results. Additional corrections can arise from the microscopic structure of the vibrational phonons, but such effects are outside the scope of the model. Nevertheless, nearly all the states of primarily octupole⊗hole structure have been populated in the (d,p) one-neutron transfer reaction [29]. The calculated wave functions show indeed small components of neutron-particle configurations in all the states under study. We summarize in Table V the information concerning experimental and calculated spectroscopic factors for these states, and the calculated $E1$ transition probabilities when all the possible contributions are taken into account. The value of the effective charge used for all the single-particle $E1$ transitions is $e_{\rm eff}=0.08$. The agreement of the calculated with the experimental $B(E1)$ values clearly improves. One notable exception is the transition from the second $5/2^+$ state, of principally $3^-\otimes f_{5/2}^{-1}$ character to the first $5/2^-$ state, of dominant $f_{5/2}^{-1}$ structure. The very reduced calculated transition probability is due to destructive interference between the core- and single-particle amplitudes.

The effective charge for a single-particle $E1$ transition is, in principle, dependent on the pair of orbitals involved. However, the structure of the states involved in the studied $E1$ transitions is not known experimentally well enough to allow for a better determination of the orbital-dependent effective charges. The spectroscopic factors are also not well enough reproduced, and the errors involved in the determination of the experimental spectroscopic factors are quite large. We have used, therefore, a common value of the effective charge for all the single-particle transitions involved. It is nonetheless of interest to study the dependence of the different calculated $E1$ transitions on the effective charge. Figure 8 shows this dependence for the transitions which were determined experimentally in this work. The shaded areas cover the interval of variation of the calculated $B(E1)$ values and are due to the uncertainty in the experimental value of $B(E1;2_1^+\rightarrow 3_1^-)$. In some cases, a large uncertainty is obtained for the calculated values, due to significant interference effects between the core and single-particle contributions to the $E1$ transition probability. The experimental values and their uncertainties are plotted with straight lines. Nearly all the experimental transition probabilities can be reproduced using an effective charge in the interval 0.01–0.14. For the transitions to which the same pair of orbitals contributes, the difference in the values of the effective charge needed to reproduce the experimental $B(E1)$ value is probably due to the discrepancies in the calculated and experimental spectroscopic factors.

V. SUMMARY AND CONCLUSIONS

The $(n,n'\gamma)$ reaction has been used to establish the low-energy level scheme of ^{207}Pb, and members of the $3^-\otimes f_{5/2}^{-1}$ sextuplet have been suggested. Transition rates for decays from a number of levels in ^{207}Pb have been determined from DSAM lifetime measurements, particularly $E1$ transitions from hole-octupole coupled states. $E3$ transition rates, where measured, are consistent with the weak-coupling picture of collective excitations in ^{207}Pb.

The particle-core model provides a rather good description of the structure of the selected states populated in the $(n,n'\gamma)$ experiment. The structure of these states agrees well with the weak-coupling expectations. Nevertheless, it was shown that the experimental $E1$ transition probabilities can only be described when the effect of small single-particle admixtures in the wave functions is taken into account.

ACKNOWLEDGMENTS

We wish to acknowledge useful discussions with K. H. Maier and M. T. McEllistrem. This work was supported by the U. S. National Science Foundation under Grant No. PHY-9803784.

[1] A. De-Shalit, Phys. Rev. **122**, 1530 (1961).
[2] Minfang Yeh, P. E. Garrett, C. A. McGrath, S. W. Yates, and T. Belgya, Phys. Rev. Lett. **76**, 1208 (1996).
[3] M. Yeh, M. Kadi, P. E. Garrett, C. A. McGrath, S. W. Yates, and T. Belgya, Phys. Rev. C **57**, R2085 (1998).
[4] C. A. McGrath, P. E. Garrett, M. F. Villani, and S. W. Yates, Nucl. Instrum. Methods Phys. Res. A **421**, 458 (1999).
[5] E. Sheldon and V. C. Rodgers, program CINDY [Comput. Phys. Commun. **6**, 99 (1973)].
[6] T. Belgya, G. Molnár, and S. W. Yates, Nucl. Phys. **A607**, 43 (1996).
[7] M. J. Martin, Nucl. Data Sheets **70**, 315 (1993).
[8] C. P. Swann, Nucl. Phys. **A201**, 534 (1973).
[9] E. Radermacher, M. Wilhelm, P. von Brentano, and R. V. Jolos, Nucl. Phys. **A620**, 151 (1997).
[10] W. P. Alford and D. G. Burke, Phys. Rev. **185**, 1560 (1969).
[11] J. C. Hafele and R. Woods, Phys. Lett. **23**, 579 (1966).
[12] A. Bohr and B. R. Mottelson, *Nuclear Structure* (W. A. Benjamin, Reading, MA, 1975), Vol. 2, p. 571.
[13] I. Hamamoto, Nucl. Phys. **A126**, 545 (1969).
[14] I. Hamamoto, Nucl. Phys. **A141**, 1 (1970).
[15] E. Grosse, C. F. Moore, J. Solf, W. R. Hering, and P. von Brentano, Z. Phys. **218**, 213 (1969).
[16] G. Vallois, J. Saundinos, O. Beer, M. Gendrot, and P. Lopato, Phys. Lett. **22**, 659 (1966).
[17] S. M. Smith, P. G. Roos, Cyrus Moazed, and A. M. Bernstein, Nucl. Phys. **A173**, 32 (1971).
[18] A. Nord, S. W. Yates, O. Beck, D. Belic, P. von Brentano, T. Eckert, C. Fransen, R.-D. Herzberg, U. Kneissl, H. Maser, N. Pietralla, H. H. Pitz, and V. Werner, Phys. Rev. C **57**, 3459 (1998).
[19] O. Häusser, F. C. Khanna, and D. Ward, Nucl. Phys. **A194**, 113 (1972).
[20] R. H. Spear, At. Data Nucl. Data Tables **42**, 55 (1989).
[21] K. Heyde and P. J. Brussaard, Nucl. Phys. **A104**, 81 (1967).
[22] K. Heyde, *The Nuclear Shell Model* (Springer-Verlag, Berlin, 1994).

[23] A. M. Oros, Ph.D. thesis, Cologne, 1996.
[24] L. Trache, K. Heyde, and P. von Brentano, Nucl. Phys. **A554**, 118 (1993).
[25] K. Heyde, P. Van Isacker, M. Waroquier, J. L. Wood, and R. A. Meyer, Phys. Rep. **102** (1983).
[26] A. Bohr and B. Mottelson, *Nuclear Structure* (Benjamin, London, 1975), Vol. II.
[27] J. Blomquist, Phys. Lett. **33B**, 541 (1970).
[28] J. Dudek, Z. Szymanski, and T. Werner, Phys. Rev. C **23**, 920 (1981).
[29] National Nuclear Data Center, Brookhaven, NY.
[30] Minfang Yeh, P. E. Garrett, C. A. McGrath, S. W. Yates, and T. Belgya (unpublished).